Journal of Materials Chemistry C

ROYAL SOCIETY OF CHEMISTRY

PAPER

View Article Online
View Journal

Cite this: DOI: 10.1039/c9tc06945c

Designing hierarchical structures of complex electronically conducting organic polymers *via* one-step electro-polymerization†

Tharindu A. Ranathunge,[a] Duong T. Ngo,[a] Dilan Karunarathilaka,[a] Nuwan H. Attanayake,[b] Indika Chandrasiri,[a] Phillip Brogdon,[a] Jared H. Delcamp,[a] R. M. Gamini Rajapakse*[ac] and Davita L. Watkins*[a]

Received 19th December 2019,
Accepted 18th March 2020

DOI: 10.1039/c9tc06945c

rsc.li/materials-c

Thermal chemical synthesis of conjugated polymers has often been plagued by low product yields, by-product contamination and high-cost catalysts. Electrochemical synthesis is an alternative strategy that can overcome these failures to obtain highly efficient syntheses. Herein, we present the study of diketopyrrolopyrrole-bisthiophene ($DPPT_2$), diketopyrrolopyrrole-bisfuran ($DPPF_2$) and thienothiadiazole-bisthiophene ($TTDT_2$) for diblock copolymerization with terthiophene (T_3) as a π-linker to form tunable narrow band gap polymers. The polymers suspended as thin films have similar redox characteristics to the monomers with potential shifts that prove the identity of the respective polymers. Electrochemical impedance measurements were carried out in the −0.6 V to 1.0 V potential range with an average electron transport resistance (R_e) value of 110 Ω irrespective of the applied potential. This confirms the polymers to have higher intrinsic electrical conductivity. The atomic ratios of the synthesized materials were calculated experimentally using energy dispersive X-ray (EDX) analysis, and they confirm the theoretical composition of the polymers. These doped polymers exhibit absorption bands in the visible to SWIR region (800–1800 nm) with optical band gaps from 0.773 to 1.178 eV in both the solid and the solution state.

Introduction

From organic electronic devices[1,2] to biomedical imaging[3,4] and sensors, application of electronically conducting polymers has helped to support a myriad of advancements in a broad spectrum of technologies.[5] The key to harnessing the unique properties that make these applications possible is in the molecular engineering of the polymer backbones. Of particular interest are conjugated polymers consisting of alternating donor (D) and acceptor (A) moieties. Such compositions have played crucial roles in polymeric conductivity,[6] photoluminescence,[7] and mechanical stability.[8] Although thermal chemical synthesis has shown promise in affording polymers with moieties or units that can be tuned to yield a wide range of functionalities, a more convenient yet atom-economic and environmentally friendly strategy towards conjugated polymers is *via* one-step electro-copolymerization.[9,10]

The area of electro-copolymerization to synthesize complex D–A materials with unique inherent properties is still in its infancy. Natera and coworkers electro-synthesized D–A polymers comprised of diphenylamine and carbazole as monomer units.[11,12] The electro-copolymerization afforded materials possessing reversible redox characteristics and electrochromic properties as well as rapid color switching abilities. Onal *et al.* developed electrochromic D–A–D polymers of polyhedral oligomeric silsesquioxane (POSS) with substituted phthalimide units as acceptor units with thiophene and 3,4-ethylenedioxythiophene (EDOT) as donor units.[13] These polymers possessed band gaps as low as 1.72 eV.

Using electro-copolymerization as a versatile tool in synthesizing alternating and block copolymers, we have designed extended conjugation monomer units with unique optical properties and excellent conductivities in comparison to conventional conjugated polymers.[14] Employing benzothiadiazole (BTD)-based motifs, the possibility of synthesizing block copolymers with perfectly controlled block stoichiometry *via* electropolymerization was demonstrated. Advancing further, D–A conjugated polymers containing diketopyrrolopyrrole (DPP) and thienothiadiazole (TTD) as acceptor units and thiophene as the donor were electro-copolymerized by taking terthiophene (T_3) as the initiator and linker to result in alternating block copolymers, poly-(T_3-$DPPT_2$) or poly(T_3-$TTDT_2$).[15] The materials were shown to possess absorption bands in the visible, NIR and SWIR regions up to

[a] Department of Chemistry and Biochemistry, University of Mississippi, University, MS 38677-1848, USA. E-mail: dwatkins@olemiss.edu
[b] Department of Chemistry, Temple University, 1901 North 13th Street, Philadelphia, Pennsylvania 19122, USA
[c] Postgraduate Institute of Science, University of Peradeniya, Kandy 20400, Sri Lanka. E-mail: rmgr@pdn.ac.lk

† Electronic supplementary information (ESI) available. See DOI: 10.1039/c9tc06945c

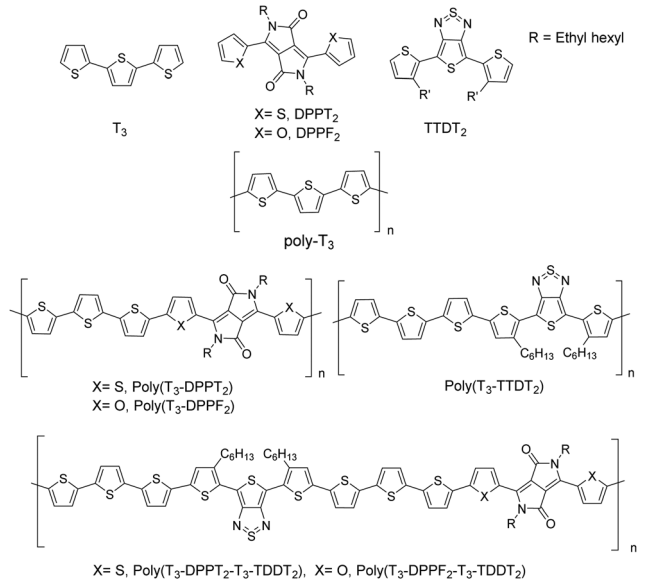

Fig. 1 Monomers and respective hypothesized structures of the polymers formed *via* electropolymerization.

1800 nm. In addition, electrochemical impedance results showed that the polymers were intrinsically conducting over a wide potential window.

The suitability of electropolymerization has not yet been fully explored in designing hierarchical architectures of polymers with highly improved electrical and optical properties. This study builds on our prior work to design copolymers containing ethyl hexyl substituted diketopyrrolopyrrole-bisthiophene ($DPPT_2$) or diketopyrrolopyrrole-bisfuran ($DPPF_2$) and thienothiadiazole-bisthiophene ($TTDT_2$) as acceptor (A (DPP-based) and A′ (TTD-based), respectively) moieties by connecting them through donor (D) moieties of terthiophene (T_3) to result in D–A–D–A′ type polymers. The resulting polymers, **poly(T_3-$DPPT_2$-T_3-$TTDT_2$)** and **poly(T_3-$DPPF_2$-T_3-$TTDT_2$)**, are illustrated in Fig. 1. Herein, we show that electropolymerization has resulted in copolymers containing all three components. By systematically analyzing the electrochemical and optical properties of the materials and comparing them with the respective diblock copolymers and T_3 homopolymer, we provide a new 3-component polymer variation on the theme of electrogenerated conjugated materials with unique properties.

Experimental

Materials

All reagents were obtained from commercial vendors and used as received unless otherwise stated. The synthetic pathways for the $DPPT_2$, $DPPF_2$, $TTDT_2$ and T_3 monomers were adopted from previously reported literature and are outlined in the ESI.†

Electropolymerization

Respective monomer mixtures of $DPPT_2$, $TTDT_2$ and T_3 for **poly(T_3-$DPPT_2$-T_3-$TTDT_2$)** or $DPPF_2$, $TTDT_2$ and T_3 for **poly(T_3-$DPPF_2$-T_3-$TTDT_2$)** were dissolved in 10.0 mL of acetonitrile such that each monomer is in a 1 mmol dm^{-3} concentration within the solution (Tables S1 and S2, ESI†). To the solution, a tetrabutylammonium hexafluorophosphate background electrolyte (BGE) was added (0.1 mol dm^{-3} concentration). Electro-polymerization, cyclic voltammetry (CV) and AC-impedance studies were performed in a one-compartment cell containing three electrodes with a glassy carbon (GC) or fluoride-doped tin oxide (FTO) working electrode (WE), a saturated calomel electrode (SCE) as the reference electrode (RE) and a Pt-wire counter electrode (CE). All potentials quoted are with respect to SCE unless otherwise stated. In each case, the solution was degassed by purging with high purity argon gas for 20 minutes and a slow flow of argon was maintained above the solution to prevent re-entry of air. Based on our previous work,[14,15] electro-copolymerization was performed *via* 10 repetitive CV cycles by selecting a potential range between 0.0 V and +1.2 V to prevent over-oxidation of the polymers. Decreasing the upper potential limit in the synthesis of **poly(T_3-$DPPT_2$-T_3-$TTDT_2$)** to +0.8 V, +1.0 V and +1.1 V did not result in polymerization and hence the range 0.0 V to +1.2 V was chosen as the minimum range for successful polymerization (*vide infra*). The polymer films obtained on the WE surface were washed with acetone to remove any small organic residue and CV and AC-impedance characteristics were recorded in argon purged neat BGE without monomers. CVs were recorded in the potential range from −2.0 V to +1.2 V to include all redox peaks of the copolymers and a scan rate of 100 mV s^{-1} was used unless otherwise indicated. P-doping was carried out from 0 V to an end potential of 1.2 V. The as formed p-type (p-doped) polymers were cycled ten times in the potential range from −1.0 V to −1.5 V to make them n-type (n-doped). The end potential for n-doping is −1.0 V. Nyquist and Bodé plots of the AC impedance characteristics were recorded in the frequency range from 0.1 Hz to 1 MHz at several selected DC potential bias values in the above potential range, which contained all the information of the electrochemical system being investigated.

Characterization

Samples were deposited and studied on fluorine-doped tin oxide (FTO) substrates. To remove any residual solvents, the samples were cleaned with acetone and dried in a vacuum oven at 50 °C prior to obtaining ultraviolet-visible-near infrared-short wavelength infrared (UV-vis-NIR-SWIR) spectra and scanning electron microscopy (SEM) images. UV-vis-NIR-SWIR spectra were measured with a Cary 5000 spectrophotometer on the samples deposited on FTO substrates. SEM images were obtained with a FEG Quanta 450 FEG electron microscope, operated at an acceleration voltage of 5 keV. A low acceleration voltage of 5 keV was chosen since polymers usually undergo burning when highly energetic electrons are incident at the high acceleration voltages of 10 keV or 20 keV normally used for robust inorganic materials. Energy dispersive X-ray spectra (EDX) and elemental maps were obtained with an X-MaxN 50 spectrometer (Oxford Instruments) mounted on the SEM.

Results and discussion

Electro-copolymerization

Fig. 2a and b show the repetitive CVs demonstrating the electro-polymerization leading to the formation of films of

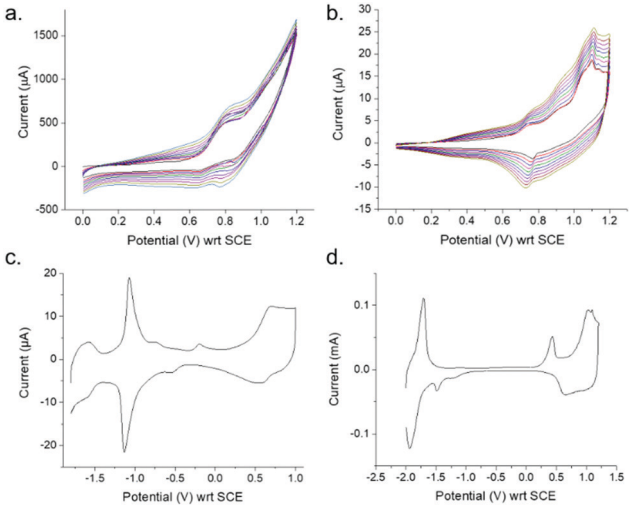

Fig. 2 CVs representing electropolymerization of (a) $DPPT_2$, $TTDT_2$ and T_3 and (b) $DPPF_2$, $TTDT_2$ and T_3 monomer mixtures leading to **poly(T_3-$DPPT_2$-T_3-$TTDT_2$)** and **poly(T_3-$DPPF_2$-T_3-$TTDT_2$)**, respectively, on a GC electrode surface. CVs of **poly(T_3-$DPPT_2$-T_3-$TTDT_2$)** and **poly(T_3-$DPPF_2$-T_3-$TTDT_2$)** in neat BGE are shown in (c) and (d), respectively.

poly(T_3-$DPPT_2$-T_3-$TTDT_2$) and **poly(T_3-$DPPF_2$-T_3-$TTDT_2$)**, respectively, on GC surfaces. The CVs of the two polymers in the neat BGE without monomers are shown in Fig. 2c and d, respectively. CVs obtained for the polymerization of the T_3-$DPPF_2$ monomer unit as well as the polymer obtained on FTO surfaces are given in the ESI† (Fig. S3–S7).

As indicated in Fig. 2a and b, an increase in current in consecutive CVs demonstrates the deposition of the conducting polymer films on the GC (WE) surface. As revealed in our previous work, both $DPPT_2$ and $TTDT_2$ can be separately copolymerized electrochemically using T_3 to result in di-block copolymers of T_3-$DPPT_2$ and T_3-$TTDT_2$.[15] Attempts to polymerize $DPPT_2$ and $TTDT_2$ separately and in a 1 : 1 mixture of $DPPT_2$ and $TTDT_2$ without T_3 in the potential range from 0.0 V to +1.2 V give no increase in current for successive CVs and no polymer films were observed on the WE surfaces (Fig. S5–S7, ESI†). Similarly, $DPPF_2$ also did not polymerize on its own in the potential range from 0.0 V to +1.2 V. The T-T-$T^{\bullet+}$ cation radicals formed during electropolymerization are potentially used as initiators and linkers to connect DPP or TTD units in the polymer chains.[15] When poly(T_3) is formed, two oxidation onsets appear: +0.639 V and +0.972 V. The first onset is due to the formation of a cation radical at each monomeric unit of the polymer (*i.e.*, poly(T-T-$T^{\bullet+}$)), and the second onset is due to the formation of a dication radical (*i.e.*, poly($^{+}$T-T-$T^{\bullet+}$)). Therefore, potentials above the second oxidation onset of T_3 are needed. This is because at higher potentials the concentration of the reactive radical species ($^{+\bullet}$T-T-$T^{\bullet+}$) is higher. In addition, these radicals possess more energy to surpass the activation energy associated with polymerization. Thus, electropolymerization was carried out at two potentials that surpass those of poly(T_3): at 0.8 V and at 1.2 V. By using these higher potentials, $^{+\bullet}$T-T-$T^{\bullet+}$ can induce the sequential oxidation of two thiophene units at both ends of the $TTDT_2$ and $DPPT_2$ monomers in the first propagation step to result in the formation of a -T-TTD-T-T_3-T-DPP-T- unit. This dication radical ($^{+\bullet}$T-T-$T^{\bullet+}$) is necessary for further propagation of polymerization. Likewise, $DPPF_2$ can be incorporated in the place of $DPPT_2$. Thus, when mixtures of T_3, $DPPT_2$ or $DPPF_2$ and $TTDT_2$ are polymerized in the potential range between 0.0 V and +1.2 V, both $DPPT_2$ and $TTDT_2$ units are presumed to be linked successively through these T_3 cation radicals.[15,16] Indirect evidence is exhibited in the CVs of polymers which contain more redox peaks than their bi-monomer counterparts (Table S3, ESI†).

The CVs of the polymers (Fig. 2c and d) obtained in BGE provide clear evidence of the three monomer units incorporated in each copolymer. In **poly(T_3-$DPPT_2$-T_3-$TTDT_2$)**, the presence of T_3 is designated by an oxidation peak at +0.692 V in the forward scan and its corresponding reduction peak appearing at +0.617 V in the reverse scan. These peaks were found to be present in the CV of poly(T_3), which appear at +0.508 V and +0.689 V, respectively, but not in the CVs of either of the monomers $DPPT_2$ and $TTDT_2$. In **poly(T_3-$DPPF_2$-T_3-$TTDT_2$)**, the peaks corresponding to poly(T_3) appear at +0.435 V and +0.654 V, respectively. The redox couple appearing at −1.134 V (cathodic peak) and −1.135 V (anodic peak) of **poly(T_3-$DPPT_2$-T_3-$TTDT_2$)** was shown to appear at −1.165 V and −1.081 V respectively in poly(T_3-$TTDT_2$). These peaks are absent in the prior report on poly(T_3) and poly(T_3-$DPPT_2$).[15] In **poly(T_3-$DPPF_2$-T_3-$TTDT_2$)**, these peaks appear at −1.105 V and −1.483 V, respectively. This electrochemical behavior proves the presence of the TTD unit in both copolymers. Our previous work shows a characteristic reduction peak for poly(T_3-$DPPT_2$) at −1.421 V which is not present in poly(T_3) but is exhibited solely by the monomeric unit, $DPPT_2$ (−1.198 V).[15] **Poly(T_3-$DPPT_2$-T_3-$TTDT_2$)** has this distinctive reduction peak at −1.577 V, a −0.156 V shift from the reduction peak observed in poly(T_3-$DPPT_2$). Since such a peak is not present in both poly(T_3) and poly(T_3-$TTDT_2$), it can be concluded that DPP has been incorporated into the backbone of **poly(T_3-$DPPT_2$-T_3-$TTDT_2$)**. In **poly(T_3-$DPPF_2$-T_3-$TTDT_2$)**, a reduction peak appearing at −1.940 V is attributed to the presence of $DPPF_2$. This peak appears at −1.905 V in poly(T_3-$DPPF_2$) (+35 mV shift, Fig. S4, ESI†) but is absent in both poly(T_3) and the $TDDT_2$ monomer and displays quasi-reversible features with its oxidation appearing at −1.708 V.

An on-going research goal has been to investigate the effects of heterocycles on semiconducting properties.[17] Just by changing the heteroatom (*i.e.*, thiophene to furan), a noticeable change in CV current is observed (Fig. 2a and b). The difference in current is due to the higher number of radicals ($^{+\bullet}$T-T-$T^{\bullet+}$) formed in the reaction propagation step for $DPPT_2$ polymers *versus* that of $DPPF_2$ polymers. We can conclude that $DPPT_2$ has a lower activation barrier for polymer propagation than that of $DPPF_2$. In turn, this affords a higher concentration of $^{+\bullet}$T-T-$T^{\bullet+}$ radicals and more $DPPT_2$-based polymer formation (*i.e.*, depositing on the electrode). The higher activation barrier for polymer propagation in the $DPPF_2$-based polymers is due to the higher charge density and charge separation stemming from the furan moiety. The higher current is presumably due to faster polymerization kinetics in $DPPT_2$.[14,18–20] Notably, the replacement of thiophene for furan units results in a much

larger negative shift in the peak positions of the DPP redox couple. Due to the difference in electronegativity between oxygen and sulfur, $DPPF_2$ results in a more polarized backbone in **poly(T_3-$DPPF_2$-T_3-$TTDT_2$)** than in **poly(T_3-$DPPT_2$-T_3-$TTDT_2$)**. This change in heteroatom yields a redox chemistry (*i.e.*, electrochemical profile) that shows more pronounced curve features in **poly(T_3-$DPPF_2$-T_3-$TTDT_2$)** than in **poly(T_3-$DPPT_2$-T_3-$TTDT_2$)** (Fig. 2c and d).

Another striking feature is that although the two polymers were grown under identical conditions, the currents in the CV of **poly(T_3-$DPPF_2$-T_3-$TTDT_2$)** are four times higher than those obtained for **poly(T_3-$DPPT_2$-T_3-$TTDT_2$)** (Fig. 2c and d). Again, this is believed to be due to an increased rate of polymerization in $DPPT_2$, yielding a higher polymer deposition of **poly(T_3-$DPPT_2$-T_3-$TTDT_2$)** than that observed for **poly(T_3-$DPPF_2$-T_3-$TTDT_2$)**. The latter, however, appears to exhibit faster redox switching in BGE than its $DPPT_2$-based counterpart.[21] Such rapid electrochemical switching occurring between p- and n-doped states for **poly(T_3-$DPPF_2$-T_3-$TTDT_2$)** is evident by the sizable increase in current as seen in Fig. 2c and d. Therefore, when the CV is recorded at the same scan rate (100 mV s^{-1}), the polymer with faster electrochemical kinetics affords higher currents.

Shifts in the peak potentials of the monomeric units in **poly(T_3-$DPPT_2$-T_3-$TTDT_2$)** and **poly(T_3-$DPPF_2$-T_3-$TTDT_2$)** from those of their parent compounds indicate that the three units are interacting with each other—presumably through a chemical attachment that leads to changes in electron densities *via* polarization of the molecules. Since T_3 is required in the electro-copolymerization to link all of the $DPPT_2$, $DPPF_2$ and $TTDT_2$ monomer units, it is therefore likely that T_3 acts as a linker to yield an arrangement of -T_3-$DPPT_2$-T_3-$TTDT_2$-T_3- and -T_3-$DPPF_2$-T_3-$TTDT_2$-T_3- *via* successive addition of either of the two acceptors units on either side of T_3. Repetition of this process of coupling through T_3 dication radicals would result in the formation of copolymers having D–A–D–A′-molecular architectures. These early electrochemical results provide evidence that both copolymers are not mixtures of their diblock counterparts but have all three monomer units in the same chain bound in close proximity. Additional supporting evidence for the formation of D–A–D–A′-type copolymers is provided *via* SEM-EDX and absorbance data analysis (*vide infra*).

Electrical properties

Noticeably, the CVs of **poly(T_3-$DPPT_2$-T_3-$TTDT_2$)** and **poly(T_3-$DPPF_2$-T_3-$TTDT_2$)** show the highest current values in the potential domain from −1.8 V to +1.2 V (Fig. 2). Conventional electronically conducting polymers (ECPs) show high current densities at their highest positive and negative potential ends due to p- and n-doping. In between these two extremes, they typically behave as insulators possessing zero current values. **Poly(T_3-$DPPT_2$-T_3-$TTDT_2$)** (Fig. S8 and S9, ESI†) and **poly(T_3-$DPPF_2$-T_3-$TTDT_2$)** (Fig. S10 and S11, ESI†) display behavior similar to that of poly(T_3-$DPPF_2$) (Fig. S12, S13 and Table S4, ESI†) as well as the previously reported polymers poly(T_3-$DPPT_2$) and poly(T_3-$TTDT_2$).[15] However, the current densities obtained in alternating block copolymers poly(T_3-$DPPT_2$) or poly(T_3-$TTDT_2$) were much lower in typical insulating regimes than those obtained for **poly(T_3-$DPPT_2$-T_3-$TTDT_2$)** and **poly(T_3-$DPPF_2$-T_3-$TTDT_2$)**. Electron density from neighbouring donor units (*i.e.*, T_5 or T_4F) on both sides of DPP and TTD tends to polarize the polymer backbone more effectively than when either of these acceptors are present on their own. This molecular composition may give rise to high electrical conductivity. The electrical properties of **poly(T_3-$DPPT_2$-T_3-$TTDT_2$)** and **poly(T_3-$DPPF_2$-T_3-$TTDT_2$)** were further studied by AC impedance. Electrical parameters obtained from AC impedance measurements are shown in Table 1 and the Nyquist plot at each applied potential is given in Fig. S8–S13 (ESI†). The dual rail transmission line model was used in analyzing the Nyquist plots (Table S4, ESI†).[22–25]

Poly(T_3-$DPPT_2$-T_3-$TTDT_2$) exhibits electrical conductivity in the −0.6 V to +1.0 V potential range with an electron transport resistance (R_e) of an average value of 110 Ω irrespective of the applied potential. The fact that the same conductivity remains when the applied DC potential bias is zero indicates that the polymer has its own intrinsic electrical conductivity that has been attained through effective polarization generating charge carriers due to its D–A–D–A′-molecular architecture. **Poly(T_3-$DPPT_2$-T_3-$TTDT_2$)** has high R_e values at the negative potential extremes where electronic conductor behavior is not observed. The double layer capacitance (C_d) values show a characteristic trend: the C_d values are low (from 1.9 to 3.8 nF) in the potential range between −0.6 V and +1.0 V with an average value of 2.9 nF. The trend in values indicates that C_d is also independent of the applied potential within this range. This is a further indication of the high electronic conductivity of the polymer.

Table 1 Electrical properties of **poly(T_3-$DPPT_2$-T_3-$TTDT_2$)** obtained from fitting AC impedance Nyquist plots to the equivalent circuit as explained in Fig. S8, S9 and S14 (ESI)

poly(T_3-$DPPT_2$-T_3-$TTDT_2$)

E (V)	R_s (Ω)	R_e (Ω)	C_d (μF)	W (μΩ)	C (μF)
−1.5	88.17	133 380	0.9823	39.14	23.73
−1.4	87.08	15 660	0.8550	35.09	28.94
−1.3	86.22	13 730	0.6925	32.12	26.96
−1.2	83.75	8165	0.5752	26.16	16.23
−1.1	81.42	7303	0.2120	26.72	13.21
−1.0	87.95	86 320	0.1540	32.10	1.512
−0.9	88.91	136 600	0.1760	31.54	1.731
−0.8	94.67	88 330	0.2849	37.61	4.639
−0.7	105.5	39 130	0.9602	59.73	3.931
−0.6	23.34	104.3	0.0019	80.69	1.335
−0.5	25.89	105.3	0.0020	66.06	1.323
−0.4	31.80	104.3	0.0021	84.02	1.296
−0.3	32.31	103.7	0.0023	78.07	1.384
−0.2	39.98	106.2	0.0028	62.55	1.365
−0.1	43.38	107.9	0.0036	86.15	1.382
0	2.37	107.9	0.0032	88.32	1.412
+0.1	43.38	107.5	0.0032	85.42	1.470
+0.2	47.38	110.1	0.0035	88.64	1.527
+0.3	49.03	110.0	0.0036	88.54	1.539
+0.4	50.15	109.4	0.0037	61.27	1.604
+0.5	49.93	110.9	0.0036	72.41	1.623
+0.6	48.31	111.9	0.0035	70.41	1.723
+0.7	45.27	112.7	0.0032	66.73	2.093
+0.8	43.82	117.3	0.0030	74.36	2.518
+0.9	40.17	115.9	0.0028	80.38	3.281
+1.0	21.34	128.8	0.0019	98.03	5.033

The C_d values are two to three orders of magnitude greater than these values when the applied potential is below −0.7 V. C_d has risen due to the capacitance generated at the electrical double layer formed between the charged polymer layer and the electrolyte in contact with the polymer layer. The Warburg impedance (W) also shows similar characteristics. It is in the range of 60 μΩ to 100 μΩ in the potential range between −0.6 V and +1.0 V and is also hardly dependent upon the applied potential. The W values are two to three times lower at potentials below −0.7 V. The low W and high C_d values at highly negative potentials indicate that the material is behaving like a redox polymer.[26,27] Hence, the redox behavior of **poly(T_3-DPPT$_2$-T_3-TTDT$_2$)** at these negative potentials dominates over its electrical conductivity. The sharp and reversible redox peaks obtained at negative potentials in the CV of **poly(T_3-DPPT$_2$-T_3-TTDT$_2$)** also support this behavior. The electronic conductivity is significant in the negative potential regime due to the presence of DPP and TTD, which also show similar redox chemistry. As such, the designed molecular architecture contributes to the electrical conductivity of the polymer in a wide range of potentials between −0.6 V and +1.0 V and a remarkable redox behavior at more negative potentials.

The electrical data for **poly(T_3-DPPF$_2$-T_3-TTDT$_2$)** are provided in Table 2 and Fig. 2. **poly(T_3-DPPF$_2$-T_3-TTDT$_2$)** possesses higher current densities (Fig. 2) and lower resistance values on average for electron transport (R_e) than **poly(T_3-DPPT$_2$-T_3-TTDT$_2$)** (Table 2). Note that the R_e values are as low as 30 Ω–60 Ω in the range from 0 V to −0.8 V where the corresponding values for **poly(T_3-DPPT$_2$-T_3-TTDT$_2$)** are ∼100 Ω. Although **poly(T_3-DPPT$_2$-T_3-TTDT$_2$)** shows similar values up to +1.0 V, **poly(T_3-DPPF$_2$-T_3-TTDT$_2$)** shows values in the range of 2000 Ω to 6025 Ω from +0.2 V to +0.6 V. The CV shows redox characteristics attributed to furan appearing in this potential range. Such a redox behavior does not exist in **poly(T_3-DPPT$_2$-T_3-TTDT$_2$)**. As the potential is increased from +0.6 V, **poly(T_3-DPPF$_2$-T_3-TTDT$_2$)** becomes heavily p-doped and consequently R_e decreases. High R_e values are seen in the negative range below −1.0 V due to the redox behavior of both TTD and DPP. As such, both polymers have low electron transport resistance throughout although the R_e values are increasing when the redox characteristics are dominating.

Table 2 Electrical properties of **poly(T_3-DPPF$_2$-T_3-TTDT$_2$)** obtained from fitting AC impedance Nyquist plots to the equivalent circuit as explained with Fig. S10, S11 and S14 (ESI)

Poly(T_3-DPPF$_2$-T_3-TDDT$_2$)					
E (V)	R_s (Ω)	R_e (Ω)	C_d (μF)	W (μΩ)	C (μF)
−1.4	12.32	3687	0.0332	415.4	2.404
−1.2	6.976	1235	0.0514	60.17	2.371
−1.0	5.791	188.7	0.1210	42.48	2.340
−0.8	11.74	60.48	0.1557	83.79	1.966
−0.6	11.74	60.47	0.1558	83.79	1.966
−0.4	11.74	60.47	0.1557	83.79	1.956
−0.2	12.50	38.10	0.2410	9.425	2.047
0	13.68	48.56	0.2062	127.4	2.456
+0.2	12.13	6205	6.112	90.09	1.345
+0.4	12.59	4399	0.0706	85.81	1.536
+0.6	10.32	2093	0.0084	64.47	2.683
+0.8	13.05	26.55	0.0332	66.81	3.985
+1.0	15.28	29.28	1.704	77.52	61.76

Elemental composition

Although electrochemical analysis provided insight into the polymer composition, further support was provided *via* SEM-EDX analysis. SEM images reveal the morphology of the polymers as films on FTO glass (Fig. 3). SEM images of bare FTO reveal grains of FTO which afford polymer growth in an epitaxial manner leading to a thermodynamic preference for globular-like structures. The atomic ratios obtained from SEM-EDX are complicated; however, elemental mapping at the macroscopic scale shows acceptable atomic levels of carbon, nitrogen, oxygen and sulfur that support copolymerization (Table 3 and Fig. S15–S18, ESI†). Table 3 presents the theoretically calculated atomic percentages of the T_3-DPPT$_2$-T_3-TTDT$_2$ and T_3-DPPF$_2$-T_3-TTDT$_2$ tetra-block copolymers. The calculated atomic percentages of the T_3, DPPT$_2$, DPPF$_2$ and TTDT$_2$ monomers, repeat units of the theoretically possible T_3-DPPT$_2$, T_3-DPPF$_2$ and T_3-TTDT$_2$ di-block copolymers, are provided in Table S5 (ESI†).

A comparison of the theoretical atomic percentages of each compound with those obtained experimentally *via* SEM-EDX shows that the atomic percentage for oxygen is over-estimated due to the FTO substrate. In lieu of increased oxygen, the carbon percentage has been under-estimated. However, the sulfur and nitrogen percentages are accurately shown. Note that for both polymers in their as-prepared positive p-type state and those that have been made negative n-type by cycling from

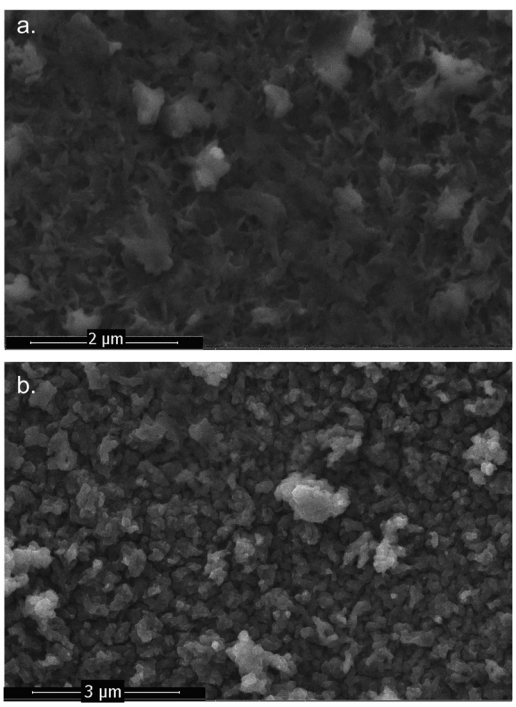

Fig. 3 Representative SEM images of (a) **poly(T_3-DPPT$_2$-T_3-TTDT$_2$)**, magnification 60 000×, and (b) **poly(T_3-DPPF$_2$-T_3-TTDT$_2$)** with a magnification of 40 000×, p-type polymers.

Table 3 Theoretically calculated and experimental average atomic percentages. Atomic averages were obtained by EDX analysis of three or four SEM images taken from different sites of the polymers grown on FTO plates

	C%	S%	N%	O%
T_3-DPPT$_2$-T_3-TTDT$_2$ p-type				
Experimental	76.50	11.70	4.10	8.00
Calculated	81.50	11.10	4.90	2.50
T_3-DPPF$_2$-T_3-TTDT$_2$ p-type				
Experimental	70.70	10.30	6.10	13.60
Calculated	81.50	8.60	4.90	4.90
T_3-DPPT$_2$-T_3-TTDT$_2$ n-type				
Experimental	76.30	10.70	4.30	10.30
Calculated	81.50	12.50	4.20	2.10
T_3-DPPF$_2$-T_3-TTDT$_2$ n-type				
Experimental	72.70	10.00	5.90	11.60
Calculated	81.50	10.40	4.20	4.20

−1.0 V to −1.5 V, the theoretical atomic percentages match closely with those of the repeat units of the tetra-block copolymers. These results therefore exclude the formation of di-block and tri-block copolymers when the three monomers are co-polymerized electrochemically. The atomic percentages match closely with tetra-block copolymers, suggesting that T_3 is required as the polymerization initiator and linker as hypothesized *via* the electrochemical and electroanalytical studies. As such, the EDX data confirm the formation of tetra-block copolymers of T_3-DPPT$_2$-T_3-TDDT$_2$ and T_3-DPPF$_2$-T_3-TDDT$_2$.

Spectroscopic studies

Fig. 4 shows the absorbance spectra for doped (*i.e.*, n- and p-type) **poly(T_3-DPPT$_2$-T_3-TTDT$_2$)** and **poly(T_3-DPPF$_2$-T_3-TTDT$_2$)** as films on FTO glass. A spectral comparison to poly(T_3-DPPF$_2$) is provided in Fig. S19 (ESI†). Energy band diagrams are provided in the ESI† (Table S6; Fig. S20–S25) where energy values were calculated using onsets of absorption bands presented in the spectra.[28,29] These absorbances correlate to the doped nature of the polymers as well as conjugated π → π* and n → π* transitions. **Poly(T_3-DPPT$_2$-T_3-TTDT$_2$)** shows an absorption peak between 360 nm and 380 nm for both the p-type and n-type polymers. However, in the p-type polymer other peaks are observed at 761 nm and 1579 nm. In contrast, the n-type polymer shows absorbance peaks at 1058 nm and 1564 nm. The spectra for **poly(T_3-DPPT$_2$-T_3-TTDT$_2$)** have shoulders near the polaron bands of the doped polymers corresponding to 1.18 eV (p-type) and 1.61 eV (n-type). The respective bipolaron optical band gaps are 0.79 eV (p-type) and 0.79 eV (n-type). In **poly(T_3-DPPF$_2$-T_3-TTDT$_2$)**, the p-type polymer has an absorbance band at 361 nm as well as bands at 805 nm and 1604 nm. The n-type polymer has absorbance bands at 474 nm, 879 nm and 1552 nm. The polaron band gaps of the doped polymers correspond to 1.54 eV (p-type) and 1.41 eV (n-type). The respective bipolaron band gaps are 0.77 eV (p-type) and 0.80 eV. These absorption bands extend throughout the NIR region and into the SWIR region (1400–3000 nm) with broad bipolaron absorption extending until about 2000 nm for both polymers in either the p-type or n-type doped state. The relative strength of the low energy bipolaron band is strong at ∼1/4 the intensity of the π–π* transition intensity. Low optical band gap materials such as these are in high demand for a range of optoelectronic applications with relatively few materials with absorption features this low in energy known based on organic conjugated polymers.

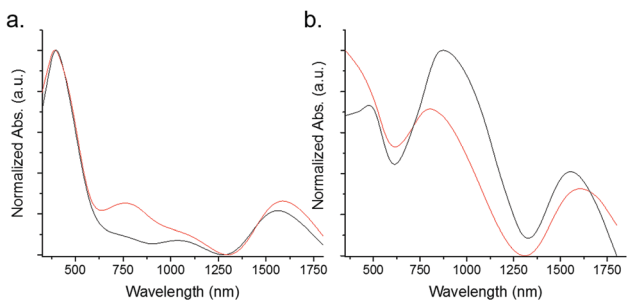

Fig. 4 Absorbance spectra of (a) **poly(T_3-DPPT$_2$-T_3-TTDT$_2$)** and (b) **poly(T_3-DPPF$_2$-T_3-TTDT$_2$)** as n-type (black) and p-type (red) variants.

Conclusions

In conclusion, this work shows the deployment of a simple electropolymerization protocol to prepare tailor-made D–A type copolymers with a D–A–D–A′ composition possessing inherent electrical conductivity in p-regimes, n-regimes, and also in between the two regimes. A comparison of electrochemical data for the monomers to that of the polymers stands as indirect evidence of co-polymerization. The elemental composition *via* SEM-EDX and variations in electrochemical behavior support the formation of D–A–D–A′ type alternating block copolymers. Compared to conventional electronically conducting polymers, the electrochemically synthesized D–A–D–A′ polymers show excellent conductivities and optical absorption bands reaching 1800 nm. These results lay the foundation for additional transformative studies in the electrosynthesis of multifaceted copolymers with potential applications in opto-electronics.

Conflicts of interest

There are no conflicts to declare.

Acknowledgements

The authors appreciate financial support of this work from the National Science Foundation under Grant Number NSF OIA-1757220. JHD and PB thank the National Science Foundation for Grant Number NSF 1455167 which supported synthesis of the TTD building block. The authors would also like to thank Dr Daniel Strongin Professor and Chair at Temple University for access to SEM-EDX.

Notes and references

1 M. V. Fabretto, D. R. Evans, M. Mueller, K. Zuber, P. Hojati-Talemi, R. D. Short, G. G. Wallace and P. J. Murphy, *Chem. Mater.*, 2012, **24**, 3998–4003.

2 T. K. Das and S. Prusty, *Polym.-Plast. Technol. Eng.*, 2012, **51**, 1487–1500.
3 T. J. Rivers, T. W. Hudson and C. E. Schmidt, *Adv. Funct. Mater.*, 2002, **12**, 33–37.
4 G. Kaur, R. Adhikari, P. Cass, M. Bown and P. Gunatillake, *RSC Adv.*, 2015, **5**, 37553–37567.
5 M. Gerard, A. Chaubey and B. D. Malhotra, *Biosens. Bioelectron.*, 2002, **17**, 345–359.
6 J. D. Yuen, J. Fan, J. Seifter, B. Lim, R. Hufschmid, A. J. Heeger and F. Wudl, *J. Am. Chem. Soc.*, 2011, **133**, 20799–20807.
7 N. S. Sariciftci, L. Smilowitz, A. J. Heeger and F. Wudl, *Science*, 1992, **258**, 1474–1476.
8 H. J. Kim, J.-H. Kim, J.-H. Ryu, Y. Kim, H. Kang, W. B. Lee, T.-S. Kim and B. J. Kim, *ACS Nano*, 2014, **8**, 10461–10470.
9 S. P. Ponnappa, S. Arumugam, H. J. Spratt, S. Manzhos, A. P. O'Mullane, G. A. Ayoko and P. Sonar, *J. Mater. Res.*, 2017, **32**, 810–821.
10 S. Hayashi and T. Koizumi, *Electrochemistry*, 2016, **84**, 570–573.
11 J. Natera, L. Otero, F. D'Eramo, L. Sereno, F. Fungo, N.-S. Wang, Y.-M. Tsai and K.-T. Wong, *Macromolecules*, 2009, **42**, 626–635.
12 J. Natera, L. Otero, L. Sereno, F. Fungo, N.-S. Wang, Y.-M. Tsai, T.-Y. Hwu and K.-T. Wong, *Macromolecules*, 2007, **40**, 4456–4463.
13 D. Çakal, S. Ertan, A. Cihaner and A. M. Önal, *Dyes Pigm.*, 2019, **161**, 411–418.
14 R. M. G. Rajapakse, N. H. Attanayake, D. Karunathilaka, A. E. Steen, N. I. Hammer, D. R. Strongin and D. L. Watkins, *J. Mater. Chem. C*, 2019, **7**, 3168–3172.
15 T. A. Ranathunge, D. Karunathilaka, D. T. Ngo, N. H. Attanayake, P. Brodgon, J. H. Delcamp, R. G. Rajapakse and D. L. Watkins, *Macromol. Chem. Phys.*, 2019, 1900289.
16 B. L. Funt and S. V. Lowen, *Synth. Met.*, 1985, **11**, 129–137.
17 M. Jeffries-El, B. M. Kobilka and B. J. Hale, *Macromolecules*, 2014, **47**, 7253–7271.
18 J. A. Del-Oso, B. A. Frontana-Uribe, J.-L. Maldonado, M. Rivera, M. Tapia-Tapia and G. Roa-Morales, *J. Solid State Electrochem.*, 2018, **22**, 2025–2037.
19 N. Elgrishi, K. J. Rountree, B. D. McCarthy, E. S. Rountree, T. T. Eisenhart and J. L. Dempsey, *J. Chem. Educ.*, 2018, **95**, 197–206.
20 D. P. Harrison, L. S. Carpenter and J. T. Hyde, *J. Visualized Exp.*, 2015, e52035, DOI: 10.3791/52035.
21 A. E. Kaifer and M. Gómez-Kaifer, *Supramolecular Electrochemistry*, John Wiley & Sons, 2008.
22 A. G. MacDiarmid and A. J. Epstein, *MRS Proc.*, 2011, **328**, 133.
23 W. J. Albery and A. R. Mount, in *Electroactive Polymer Electrochemistry: Part 1: Fundamentals*, ed. M. E. G. Lyons, Springer US, Boston, MA, 1994, pp. 443–483, DOI: 10.1007/978-1-4757-5070-6_4.
24 W. J. Albery and A. R. Mount, *J. Chem. Soc., Faraday Trans.*, 1994, **90**, 1115–1119.
25 J. Heinze, B. A. Frontana-Uribe and S. Ludwigs, *Chem. Rev.*, 2010, **110**, 4724–4771.
26 K. Qu, M. Fang, S. Zhang, H. Liu and X. Zeng, *Polymers*, 2018, **10**, 1191.
27 G. Inzelt, *Electrochim. Acta*, 1989, **34**, 83–91.
28 K. M. Molapo, P. M. Ndangili, R. F. Ajayi, G. Mbambisa, S. M. Mailu, N. Njomo, M. Masikini, P. Baker and E. I. Iwuoha, *Int. J. Electrochem. Sci.*, 2012, **7**, 11859–11875.
29 W. Huang and A. MacDiarmid, *Polymer*, 1993, **34**, 1833–1845.